日本原子力研究開発機構機関リポジトリ

Japan Atomic Energy Agency Institutional Repository

Title	Evaluation of titanium vacuum chamber as getter pump
Author(s)	Kamiya Junichiro, Takano Kazuhiro, Yuza Hiromu, Wada Kaoru
Citation	e-Journal of Surface Science and Nanotechnology, 20(2), p.107-118
Text Version	Published Journal Article
URL	https://jopss.jaea.go.jp/search/servlet/search?5074378
DOI	https://doi.org/10.1380/ejssnt.2022-017
Right	Copyright: ©2022 The author(s) Published by The Japan Society of Vacuum and Surface Science

Evaluation of Titanium Vacuum Chamber as Getter Pump

Junichiro Kamiya,[1, †]   Kazuhiro Takano,[1]   Hiromu Yuza,[1]   Kaoru Wada [1, 2]

[1] *Japan Atomic Energy Agency, J-PARC Center, 2-4 Shirakata, Tokai, Naka, Ibaraki 319-1195, Japan*
[2] *Tokyo Electronics Co., Ltd., 2-22-7 Honcho, Kokubunji, Tokyo 185-0012, Japan*
[†] *Corresponding author: junichiro.kamiya@j-parc.jp*

Methods for removing the surface oxide film have been investigated to make a titanium vacuum chamber itself act as a getter pump. The build-up test of the titanium chamber has been performed to investigate the effect of baking. The result showed that the higher the baking temperature the lower the pressure rise during the build-up. Especially the baking at 400°C, the pressure kept less than 10^{-3} Pa after 2 h of build-up. The lower pressure rise in the build-up test of the vacuum-fired titanium chamber suggests that once the surface oxide has been removed by the high temperature such as 850°C in the high vacuum furnace, the surface oxide film can be removed more easily because the regenerated oxide film is thinner than before. The results of the X-ray photoelectron spectroscopy supported these facts; namely, it is shown by the photoelectron spectrum of Ti 2p near the surface that the titanium oxide peak intensity decreases while that of the metal titanium increases by the 400°C baking; the O 1s peak intensity becomes smaller near the surface while that in the bulk becomes larger by the 400°C baking, which implies the thermal diffusion of the oxygen to the bulk; the O 1s peak intensity is reduced near the surface by the vacuum firing. The effect of the removal of the surface oxide film by the sputtering has also been investigated by a throughput method. After sputtering the surface of the titanium chamber, the pressure in the titanium chamber has become lower than that in the chamber of the other side of the orifice, which is pumped by the turbomolecular pump. A large pumping speed was obtained for CO, O_2, and CO_2. Furthermore, the titanium chamber, which is non-evaporable getter (NEG) coated after sputtering the surface titanium oxide film, has been developed to prevent the pumping speed from decreasing by the repeated air exposure and activation process. The result showed the final pressure has not deteriorated even after more than 10 times air exposure and activation. This fact indicated that the surface oxide on the NEG coating would diffuse into the titanium bulk because there is no oxide barrier between the NEG coating and the titanium vacuum chamber.

Keywords *Titanium vacuum chamber; Surface oxide film; Diffusion; Sputtering; NEG coating*

I. INTRODUCTION

Titanium is used as the vacuum material especially in high-power beam accelerators due to its low radio activation characteristic [1] and low outgassing rate [2]. For example, the beam pipes and bellows are made of titanium in Japan Proton Accelerator Research Complex (J-PARC) [3, 4]. Titanium is a well-known getter material for gas molecules [5]. However, the ordinal titanium surface has no getter function because it is covered with a titanium oxide film. We have considered that the titanium vacuum chamber, including titanium beam pipes, bellows, etc., itself can be a getter pump if the surface oxide film is removed. Thus, methods to
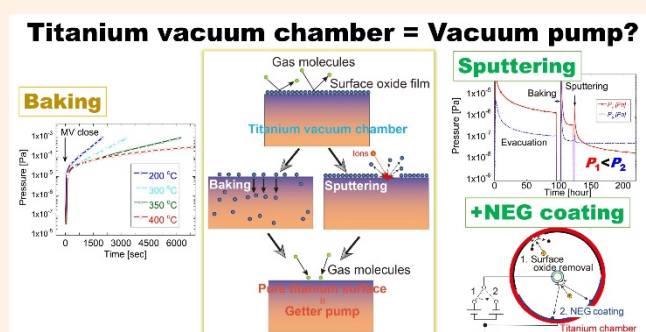
remove the surface oxide film of the titanium chamber have been investigated. Figure 1 shows the conceptual diagram of the methods to reduce or remove surface titanium oxide. One method is diffusing the surface oxide into the bulk of the chamber wall by raising the temperature of the titanium chamber, e.g., baking. The other is removing away the surface titanium oxide film by sputtering. For the baking effect, Benvenuti *et al.* investigated the coatings of the candidate elements and alloys of non-evaporable getter (NEG) coating [6−8]. As a guide to see the degree of activation, they measured the dependence of the pressure increase induced by the electron bombardment on the baking temperature. The titanium coating was one of the measuring objects. As a result,
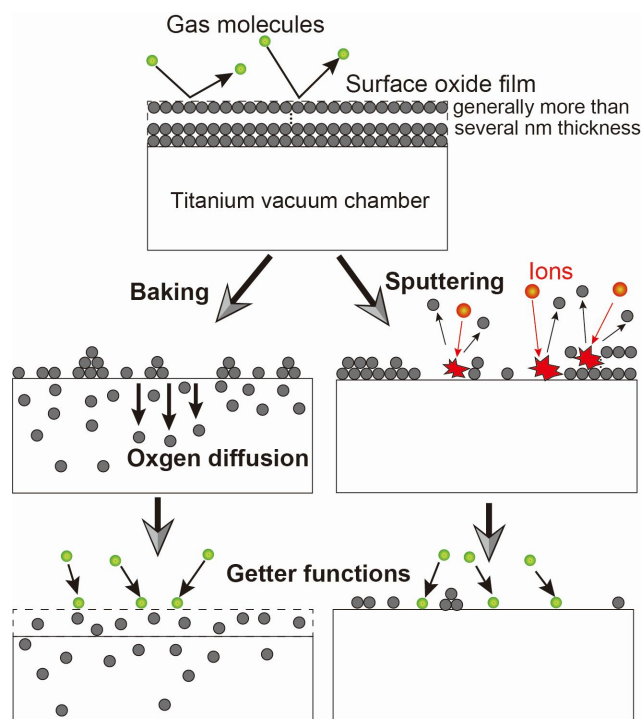
Figure 1: Conceptual diagram of the methods for removing the surface titanium oxide film to make a titanium vacuum chamber a getter pump.

the pressure increase for the titanium coated chamber is suppressed to about 1/15 by the 300°C baking and about 1/4000 by the 400°C baking compared with the 160°C baking. Recent research showed the titanium coating maintains the getter function even after the repeating air exposure and activation cycles. Miyazawa *et al.* demonstrated that the pumping speeds of the titanium coated stainless steel chamber, which is covered by the thin palladium coating on the titanium coating, did not decrease after 6 times venting and 185°C baking cycles [9]. Ono *et al.* [10] and Mase *et al.* [11] revealed that the high-purity titanium coating maintains its pumping performance even after 30 times cycles of air exposure and 185°C baking when the chamber was vented by the high purity N_2. These results had motivated us to investigate whether a titanium vacuum chamber had a getter function by baking.

For the sputtering effect, a sputter ion pump is a well-known vacuum pump, which uses the getter characteristic of titanium. During the sputter ion pump operation, the ions of the residual gas molecules hitting the titanium cathode are partially implanted in the cathode. Some of the ions sputter the titanium atoms of the cathode. Then, the titanium atoms are deposited on the surrounding materials, such as an anode. Thus, fresh titanium appears on the sputtered cathode and deposited materials [12]. We considered that the fresh titanium surface ought to appear by sputtering away the surface oxide film of the titanium vacuum chamber. A fresh titanium film surface typically has an initial sticking coefficient of about 0.06 and 0.7 for H_2 and CO, respectively, at

room temperature [5]. The corresponding pumping speed per unit area is 2.6×10^{-3} and 8.2×10^{-3} m^3 s^{-1} cm^{-2} for H_2 and CO, respectively, at room temperature. For example, when a titanium chamber has the size of 100 mm in diameter and 200 mm in length, the pumping speed is ideally about 1.7 m^3 s^{-1} for H_2 and 5.2 m^3 s^{-1} for CO, respectively. These large pumping speeds have motivated our research for giving a titanium vacuum chamber a getter function by sputtering the inner surface.

This study aims to investigate the effect of the methods for removing the surface titanium oxide film on making a titanium chamber a getter pump based on the experimental results. The preliminary results have been reported in the previous conference proceedings [13, 14]. This article includes the results of the more systematic experiments, the quantitative measurements, and the detailed considerations. First, the effect of baking on the activation of the titanium chamber is examined. Next, the effect of the removal of the surface oxide film by the direct current (DC) magnetron sputtering is described. Even if the surface titanium oxide film is removed by the above methods, it will be again formed by the air exposure of the chamber. The development for regaining the getter function even after the air exposure is undergoing. The current status of the development is also presented.

II. BAKING EFFECT FOR THE TITANIUM CHAMBER ACTIVATION

To investigate whether a titanium vacuum chamber has a getter function by baking, the build-up test of the titanium vacuum chamber was performed after baking at different temperatures. In addition, changes in the chemical composition of titanium due to the baking at different temperatures have been measured by X-ray photoelectron spectroscopy (XPS).

A. Build-up test of a titanium vacuum chamber

Figure 2 shows the system diagram of the setup for the build-up test. A titanium vacuum chamber was attached to the stainless steel vacuum chamber for pumping, which was evacuated by a turbomolecular pump (TMP; TG900M, Osaka Vacuum) with a dry scroll pump (DSP; ISP250-C, ANEST IWATA) as the fore-pump, through a metal angle valve (MV; 57.0 XHV All-Metal Angle Valve, VAT). The size of the titanium chamber was 100 mm in inner diameter and 240 mm in length. The body and ports of the titanium chamber were made of Japanese Industrial Standards (JIS) grade 2 pure titanium. The flanges were ConFlat® type. To prevent the knife edge from being rounded by pressing the gasket, the flanges were made of JIS grade 60 titanium alloy, which was widely known as Ti-6Al-4V, whose mechanical strength is much higher than that of pure titanium. The chamber surface was mechanically polished by buffing #400, chemically polished with a mixed liquid of HNO_3 and HF
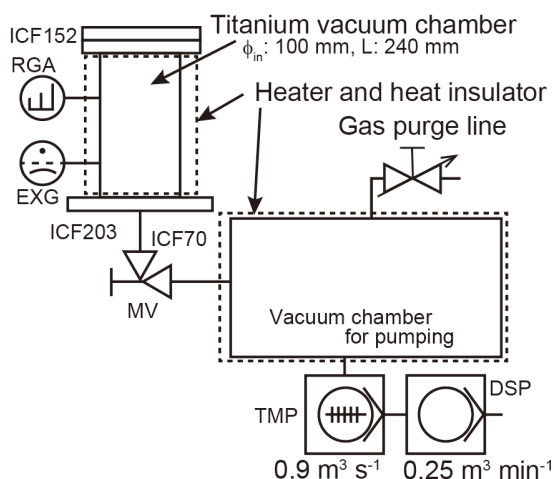
Figure 2: Schematic of the apparatus used for the build-up test. TMP is a turbomolecular pump, DSP is a dry scroll pump, EXG is an extractor gauge, RGA is a residual gas analyzer, and MV is an all-metal angle valve.

solutions, and rinsed by demineralized water in the final process of manufacturing. The thickness removed by the chemical polishing was about 15 μm. The extractor gauge (EXG; AxTRAN of model ISX2 controller with X-11 sensor head, ULVAC) and residual gas analyzer (RGA; BGM2-102, ULVAC) were installed in the ports of the titanium chamber. The EXG has been calibrated by the manufacture. The controller was calibrated by the electrical transmitter, while the sensor head was calibrated by comparing it with the standard pressure gauge using nitrogen gas. The calibration of the RGA for the typical gas species was described later.

The build-up test was performed by closing the MV. The total pressure and residual gas ion current were measured by the EXG and the RGA, respectively, which were installed in the ports of the titanium chamber. The build-up test was performed for 120 min in maximum or until the total pressure reaches 10^{-3} Pa. First, the system was pumped by the TMP with the MV open from the atmospheric pressure. After the evacuation for 1 day, the titanium chamber was baked at 200°C. Then, the build-up test was performed at room temperature by closing the MV. After opening the MV, the chamber was baked at 300°C. The same process was repeated to the build-up test after the baking at 400°C. The temperature of the chamber was 21−24°C in the build-up tests. The baking time was 8 h in 200°C baking, while it was 3 h for baking at higher temperatures. The reason for the longer baking time at 200°C is that it also functions as degassing especially for H_2O. H_2O was the main outgassing component in the 200°C baking after evacuation from the atmospheric pressure. But H_2O was reduced by this 200°C baking and the main component was H_2 and CO during the baking at the higher temperature. In the following baking at 300−400°C, the main outgassing component was H_2, and the second and third main outgassing components were CO and argon, respectively. During the baking of the titanium
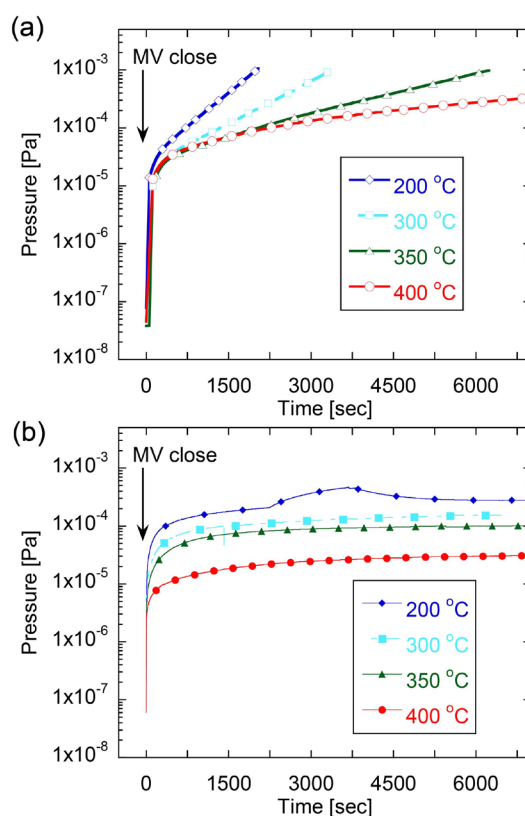

Figure 3: Build-up result of the total pressure in the titanium chamber after baking at each temperature of (a) the brand-new titanium chamber and (b) the vacuum-fired titanium chamber.

chamber, the vacuum chamber for pumping was also baked at about 150°C. A set of build-up tests, which means the above-described tests from 200−400 ℃ baking, was firstly performed for a brand-new titanium chamber. After the build-up tests, the titanium chamber was thermally treated in the vacuum furnace, which is the process known as vacuum firing [15]. The condition of the vacuum firing was 850°C for 10 h under a pressure less than 10^{-3} Pa. The furnace was evacuated by the three TMPs of 3 m^3 s^{-1} pumping speed and a cryopump of 10 m^3 s^{-1}. The DSP of 0.5 m^3 min^{-1} pumping speed was installed in each TMP fore-line. H_2 was the main outgassing component during the vacuum firing at 850°C. We assume that most of the oxygen in the titanium oxide film would diffuse to the titanium bulk by this vacuum firing. The build-up test was again performed with the vacuum-fired titanium chamber. The surface roughness was estimated with the titanium sample, which was treated in the same surface polishing and vacuum firing procedure. The sample was measured by the surface roughness meter (Surftest SJ-310, Mitutoyo). The surface roughness of the samples without vacuum firing was around 0.05−0.1 μm in the arithmetical mean deviation R_a and around 0.4−0.9 μm in the maximum peak-to-valley height R_z. That with vacuum firing samples was 0.2−0.8 μm in R_a and 1.1−4.4 μm in R_z. The surface roughness increased by the vacuum firing.
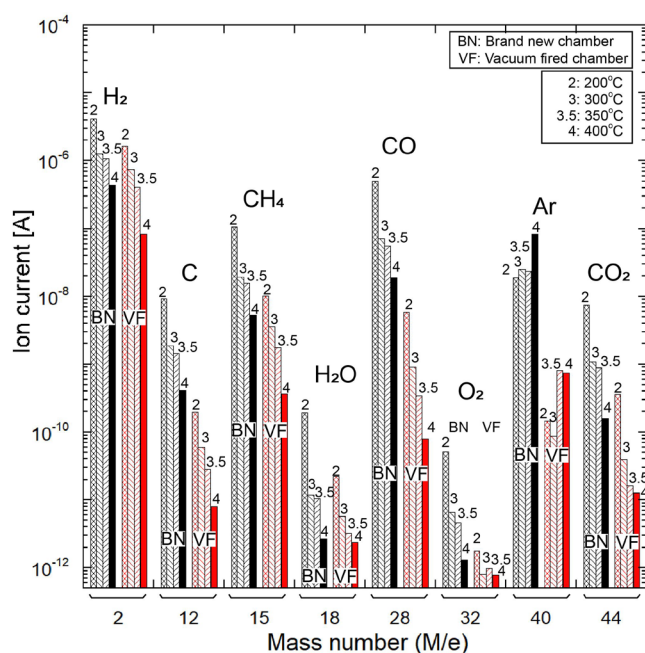
Figure 4: Ion current for each gas species after the 30-min build-up for the brand-new and vacuum fired titanium chambers. The numbers 2, 3, 3.5, and 4 in the histogram represent the baking temperatures of 200, 300, 350, and 400°C, respectively.

Figure 3(a, b) shows the result of the total pressure during the build-up for the brand-new titanium chamber and the titanium chamber with vacuum firing treatment. For the brand-new titanium chamber, the pressure reaches 10^{-3} Pa for 30, 55, and 103 min after 200, 300, and 350°C baking, respectively. Only the pressure after 400°C baking keeps under 10^{-3} Pa in 120 min build-up test. For the vacuum-fired chamber, the pressures are maintained at less than 10^{-3} Pa for all bakeout temperatures. The summary of the result is as follows: (1) The higher the baking temperature, the smaller the pressure increase for both the brand-new and vacuum fired chamber. (2) The pressure increase of the titanium chamber after vacuum firing is smaller than that without vacuum firing. (3) Relatively large suppression of the pressure increase is observed in the result of the 400°C baking. As described in Section I, the pressure increase by the electron bombardment was reported by the CERN group [6−8] for the chambers which were coated by the NEG materials. The titanium-coated chamber showed a lower pressure increase than the stainless steel chamber by 2 orders of magnitude after 400°C baking. The results of the build-up test are consistent with the CERN's results [6−8].

Figure 4 shows the amount of each gas species, which was measured by the RGA, after 30 min of build-up for the brand-new and vacuum-fired titanium chamber. The vertical axis is an ion current. The conversion factor from the ion current of the corresponding mass number to the partial pressure was measured by introducing high-purity gases (H_2, CH_4, CO, O_2, Ar, and CO_2) from the purge line and comparing the ion current of the RGA and the total pressure value

of the EXG, which was corrected by the relative sensitivity for each gas. The conversion factors are 247 Pa A^{-1} for H_2 ($M/e = 2$), 398 Pa A^{-1} for CH_4 ($M/e = 15$), 265 Pa A^{-1} for CO ($M/e = 28$), 378 Pa A^{-1} for O_2 ($M/e = 32$), 217 Pa A^{-1} for Ar ($M/e = 40$), and 364 Pa A^{-1} for CO_2 ($M/e = 44$). The same result as the total pressure is shown for all the gas species except argon. Baking at high temperatures does not decrease the amount of argon in the build-up. The increase of argon during the build-up is also reported in the recent research about the Ti-deposited SS304L chamber [10, 11]. Although the exact reason is not clear, one of the possible reasons is assumed as the following. The reduction reaction is performed under the high-temperature argon atmosphere in the titanium manufacturing process [16]. During such an atmosphere, argon diffuses into the titanium bulk. In the experiment, argon inside titanium diffuses out by the baking and becomes a residual gas in the chamber. Because argon does not stick to the titanium surface even the chamber is activated by the baking, it increases during the buildup.

B. Chemical composition analysis

To see what happens in the surface or bulk of titanium by baking, the chemical compositions have been measured by XPS (Quantera SXM, ULVAC-PHI). Sample plates of pure
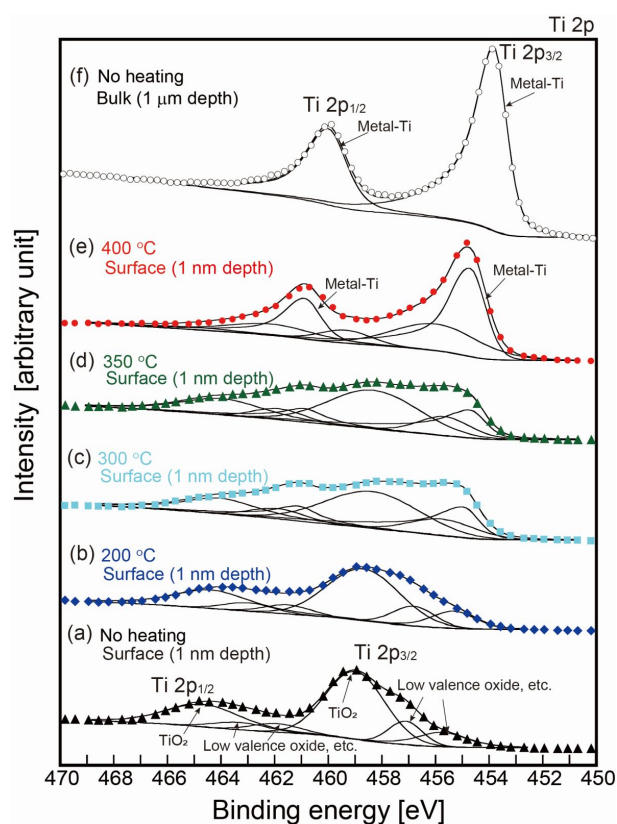

Figure 5: Ti 2p photoelectron spectra. (a) The surface (1 nm depth) of the unheated titanium sample. (b−e) The surfaces (1 nm depth) of the heated samples at 200, 300, 350, and 400°C. (f) The bulk (1 μm depth) of the unheated sample.
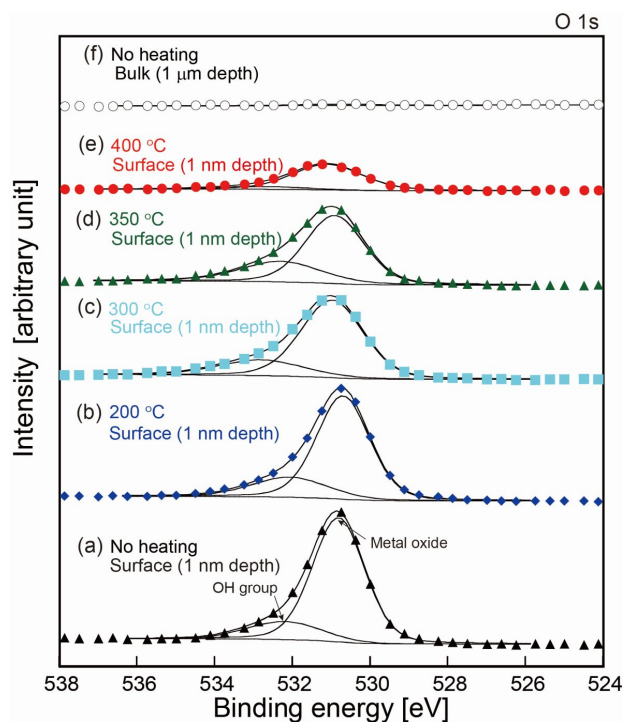
Figure 6: O 1s photoelectron spectra. (a) The surface (1 nm depth) of the unheated titanium sample. (b−e) The surfaces (1 nm depth) of the heated samples at 200, 300, 350, and 400°C. (f) The bulk (1 μm depth) of the unheated sample.
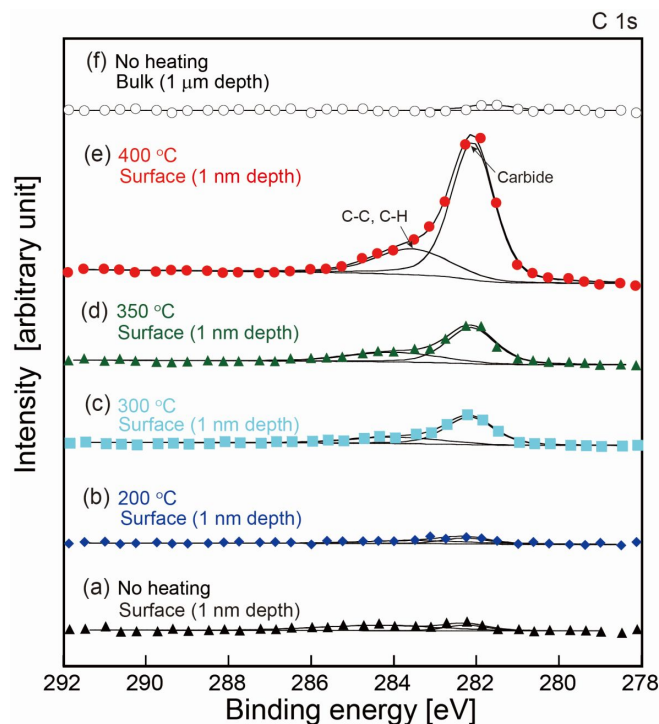

Figure 7: C 1s photoelectron spectra. (a) The surface (1 nm depth) of the unheated titanium sample. (b−e) The surfaces (1 nm depth) of the heated samples at 200, 300, 350, and 400°C. (f) The bulk (1 μm depth) of the unheated sample.

titanium (JIS Class 2) with 1 mm thickness were prepared. The titanium samples were chemically polished and rinsed by demineralized water, as was the titanium chamber. The energy resolution of the XPS apparatus was less than 0.5 eV for Ag $3d_{5/2}$. The sample was irradiated with monochromatic Al Kα X-rays with a diameter of about 200 μm. Ar^+ ions with an acceleration voltage of 1 kV were injected for sputtering to measure the depth profiles. The sputtering rate was 2.5 nm min^{-1} as the SiO_2 equivalent value. The sample stage in the sample chamber was equipped with a heating mechanism of up to 400°C.

A sample was installed in the sample chamber and evacuated to around 1×10^{-5} Pa. Next, the sample was moved to the measuring chamber with a pressure of 3×10^{-7} Pa, and the XPS measurement was performed. The sample was, then, moved to the sample chamber, and heating of the sample at a certain temperature was performed for 22 h. After the sample became room temperature, it was again moved to the measuring chamber, and the XPS measurement was performed. The different spots of the same sample were measured before and after the heating to see the chemical composition change by the heating. This process was performed *in-situ*. The heating of the sample was performed at 200, 300, 350, and 400°C.

Figure 5 shows Ti 2p photoelectron spectra. Figure 5(a) is a spectrum at the surface of 1 nm depth of the unheated titanium sample. Figure 5(b−e) corresponds spectra at the surface of 1 nm depth of the samples heated at each tempera-

ture. Figure 5(f) is a spectrum in the bulk of 1 μm depth of the unheated sample. Figures 6 and 7 show photoelectron spectra of O 1s and C 1s core levesl, respectively. The conditions of panels (a−f) are the same as those in Figure 5. Figures 8 and 9 show the depth distribution of the O 1s and C 1s peak intensities, respectively. In Figures 5−9, the representative data of the unheated samples is plotted because the data for the unheated case was almost the same for every sample.

In the bulk of 1 μm depth as shown in Figure 5(f), each peak for the Ti $2p_{3/2}$ and $2p_{1/2}$ core levels is fitted by an asymmetric function, assuming only the metallic titanium exists. Each peak is located at the binding energies of 453.9 and 460.1 eV. These binding energies are consistent with the previous reports [17−19]. The Ti $2p_{3/2}$ and $2p_{1/2}$ spectra in Figure 5(a−e) are fitted by some functions on the assumption of the existence of some kinds of titanium oxides, carbides, nitrides, metal titanium, etc. In Figure 5(a), the Ti $2p_{3/2}$ and $2p_{1/2}$ peak positions of the main fitting functions are 459.1 and 464.8 eV, respectively. This means that the main component in the surface of the unheated titanium sample is titanium oxide (TiO_2), because the binding energies are consistent with those found in literature [17, 18]. There are small peaks in the lower binding energies. They are attributed to the mixture of metallic titanium, low valence titanium oxides such as Ti_2O_3 and TiO, or titanium carbide (TiC) according to the previous research [17−19]. The binding energies of the spectra appear to be shifted to
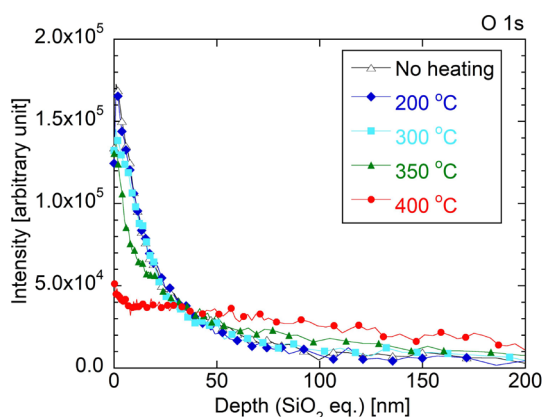
Figure 8: Depth distribution of the O 1s peak intensity for the unheated titanium sample and those heated at each temperature.
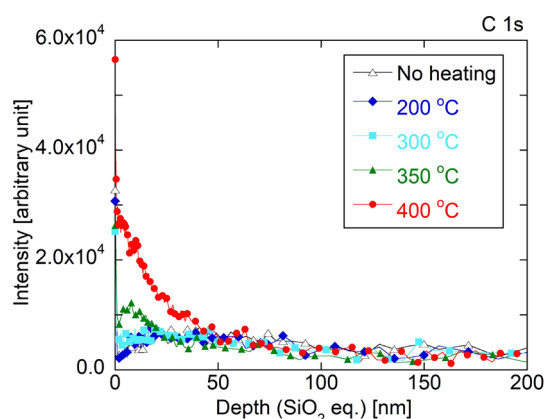

Figure 9: Depth distribution of the C 1s peak intensity for the unheated titanium sample and those heated at each temperature.

the lower binding energy side by the higher temperature heating [Figure 5(b−e)]. This is because the TiO$_2$ peaks decrease, while the peak intensity of the lower binding energy components increases. In Figure 5(e), the Ti 2p$_{3/2}$ and 2p$_{1/2}$ peak positions of the main fitting functions after 400°C heating are 454.8 and 460.9 eV, respectively, which are near the metal titanium binding energies shown in Figure 5(f). This result implies that the surface oxide layer of titanium is reduced to metallic titanium more efficiently by the higher temperature heating, which is consistent with the O 1s results (Figure 6). The small difference of the main peak positions between Figures 5(e) and 5(f) and the shoulder remaining at the higher binding energy side in Figure 5(e) may attribute to low valence titanium oxides or TiC. Especially, a larger contribution of TiC larger by higher temperature heating is expected from the C 1s results (Figure 7), which will be discussed below. The previous research [20] suggests that the Ti 2p$_{3/2}$ and 2p$_{1/2}$ peaks of TiC are 454.7 and 460.7 eV, respectively, which agree well with those of the present result.

In Figure 6, the O 1s spectra are fitted with two functions corresponding to metal oxides and hydroxide groups under the assumption that hydroxide groups and metal oxides exist [17, 18]. The peak at 531 eV corresponds to a metal oxide and that with 532−533 eV may correspond to the hydroxide groups. Figure 6 represents that the higher the heating temperature, the lower the intensity of the metal oxides near the surface. This result is consistent with Figure 5, where the peak intensity of TiO$_2$ near the surface decreases by the higher temperature heating. From Figure 8, the thickness of the surface oxide film is about 10 nm for unheated titanium, considering that the sputtering rate of titanium oxide is nearly half of that of SiO$_2$ [21]. The previous research reported the oxide film thickness of the pure titanium surface and its alloy with different surface treatments, which were measured by the transmission electron microscope (TEM) [22]. The reported thickness is from about 5 to 50 nm depending on the surface treatments. The estimation of the surface oxide film thickness from Figure 8 is consistent with

those measured by the TEM measurement. By the higher temperature heating, the O 1s intensity on the surface decreases while that in the bulk increases (Figure 8). This represents that oxygen in the surface titanium oxide diffuses into the deeper bulk of titanium by a higher temperature heating.

The C 1s spectra in Figure 7 are fitted with two functions corresponding to metal carbides and carbon contamination under the assumption that TiC and C−C, C−H, and C−O bonds of carbon contamination exist [17−19]. The peak with the binding energy of 282 eV corresponds to TiC, and that around 283−285 eV is attributed to the C−C, C−H, and C−O bonds. The intensity of TiC increases by the higher temperature heating. This result is consistent with Refs. 17−19. From Figure 9, it is noticed that the C 1s intensity increases in the deep bulk region as well as on the surface by the higher temperature heating, especially 400°C. To investigate
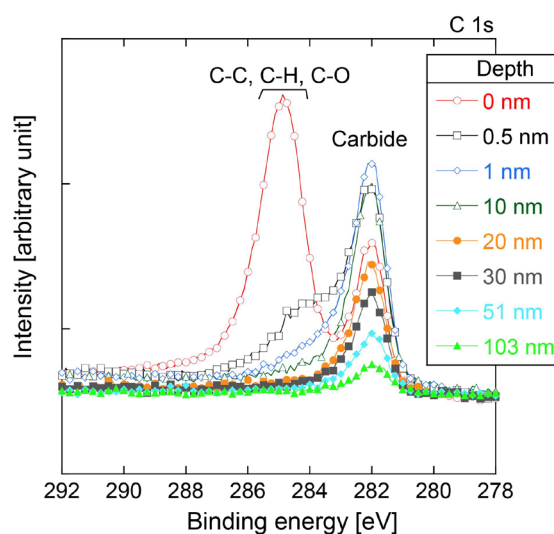

Figure 10: Depth variation of the C 1s spectra from top surface (0 nm) to about 100 nm depth for the titanium sample heated at 400°C.

Table 1: Chemical composition of the surface of the titanium samples with and without vacuum firing.

Composition	Ti without vacuum firing (at%)	Ti with vacuum firing (at%)
C	1.2	0.9
O	66.8	63.2
Ti	32.0	36.0

the carbon behavior in more details, the variation of the C 1s spectra from the top surface to about 100 nm depth is compared (Figure 10). On the top surface (0 nm), a large peak is observed at about 285 eV, which is attributed to the C−C, C−H, and C−O bonds of surface contamination [18]. This peak may include graphene because of the agreement of their binding energy (284.7 eV) [20]. The intensity of this peak drastically drops at the depth of 1 nm or deeper, and TiC becomes the main composition. These results indicate that, by the higher temperature heating, the top titanium surface is polluted by carbon contamination and carbon diffuses from the surface to a depth of a few tens nm, leading to the TiC formation. This carbon contamination on the top surface and the carbide near the surface would suppress the getter function of the titanium surface.

The surface XPS analysis has been reported for the porous titanium coating and porous and dense Ti-Zr-V NEG coatings [17, 23]. In these preceding studies, the shift of the Ti 2p peaks from the TiO_2 position to the metallic titanium position is observed by raising the temperature, which is consistent with our present study. However, the temperatures where the metallic titanium peaks are observed is different; 250°C for the porous titanium coating and 160°C for both the porous and dense NEG coating, both of which are lower that that found for the titanium plate in the present study.

The XPS analysis of the vacuum-fired titanium sample was also performed to investigate the difference of the build-up results between the titanium chamber with and without vacuum firing, The chemical composition of the surface is shown in Table 1. There is no large difference between the chemical composition of the surfaces of the non-vacuum-fired titanium and the vacuum-fired one. The amount of oxygen is large even on the surface of the vacuum-fired titanium sample. It is considered that the titanium oxide film is formed again on the surface by the air exposure after it was removed by the vacuum firing process. Figure 11 shows the comparison of the depth distribution of the O 1s peak intensity for the titanium samples with and without vacuum firing. It was found that the O 1s peak intensity becomes smaller near the surface by the vacuum firing.

As a summary of this section, the situation of the activation of the titanium chamber by baking is supposed as follows: The brand-new titanium chamber has a relatively thick surface oxide film, whose thickness is a few tens of nm. The higher temperature heating such as 400°C allows the oxides to diffuse deeper into the bulk. It means that a fraction of the titanium metal on the surface increases more by the higher
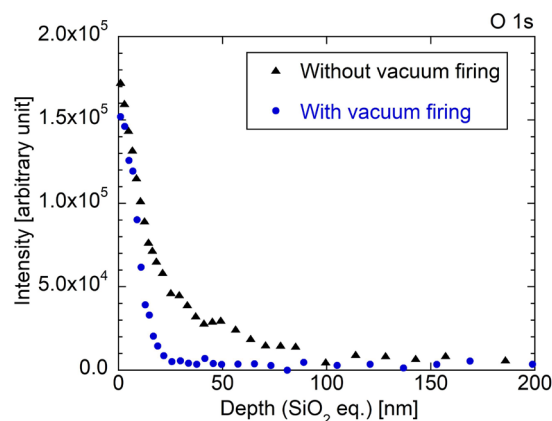

Figure 11: Depth distribution of the O 1s peak intensity for the titanium samples with and without vacuum firing. The *in-situ* heating was not performed for both samples.

temperature heating. On the other hand, the higher temperature baking of the titanium chamber results in a lower outgassing rate in the sense of the general degassing procedure. The result of the build-up test [Figure 3(a)] represents the combination of activation and the outgassing reduction. However, the oxides near the surface do not completely disappear from the surface even by baking at 400°C, and what is worse, carbon contamination and carbide increase on the surface by the higher temperature baking (Figures 6−8). These oxides and carbides near the surface would suppress the getter function of the titanium surface. Thus, the titanium chamber has been partially activated at 400°C or lower temperatures. Once the surface is almost completely composed of fresh titanium by the vacuum firing, the surface oxide film, which is again formed by the air exposure, is thinner than that of the brand-new titanium chamber (Figure 11). Then, the titanium chamber with vacuum firing can be activated at a lower temperature than that without vacuum firing. Of course, the higher the baking temperature, the higher the degree of activation, and at the same time, a more effective outgassing reduction. This is the situation shown in Figure 3(b).

III. SURFACE OXIDE REMOVAL BY SPUTTERING

A. Setup for sputtering and method of pumping speed measurement

Effectiveness of sputtering was verified as a method for removing a surface oxide film without rising the temperature. Figure 12 shows the experimental setup. The titanium chamber, whose size is the same as that used in the build-up test, was installed. The titanium chamber was connected with a stainless steel chamber through the orifice with a 17 mm diameter. There are several roles for the orifice. The first is to pump the gases, which do not stick to titanium such as rare gases and CH_4, through the orifice. A TMP
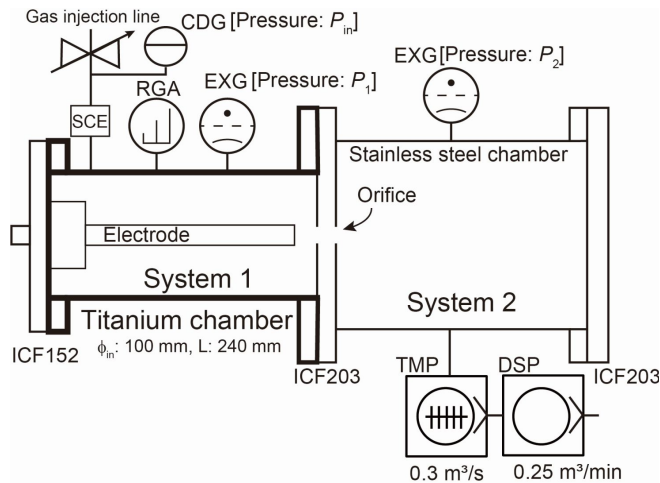
Figure 12: Setup for examining the surface oxide film removal by the sputtering. Systems 1 and 2 are connected with the orifice. Only system 2 is evacuated by the TMP. CDG is a capacitance diaphragm gauge, and SCE is a standard conductance element.

(STP-iX455, Edwards) and a DSP (ISP250-C, ANEST IWATA) were used for a main pump and a fore-pump, respectively. The second role is to demonstrate the pumping ability of the titanium chamber by comparing the pressures of both sides of the orifice. The third is to measure the pumping speed by the throughput method. The total pressure in each system was measured by an EXG (IE 514 sensor, IONIVAC IM540, Leybold). A RGA (BGM2-102, ULVAC) was installed in system 1 to check the residual gas composition. The pressures measured by the EXG were corrected with the relative sensitivities to different gasses, which were given by the manufacturer. The gas inlet line was connected to system 1. The inlet gas pressure was measured by a capacitance diaphragm gauge (M-342DG, CANON ANELVA). The standard conductance element (SCE) was used to fix the conductance of the gas inlet line [24]. A cylindrical electrode with a diameter of about 20 mm was inserted in the central axis of the titanium chamber. In the electrode, neodymium magnets were arranged to effectively make the plasma. Argon was used for sputtering gas. A DC voltage of about +0.3 kV was applied to the electrode during the sputtering. The chamber was connected to the ground potential. The sputtering rate was roughly estimated to be 1 nm min^{-1}. The

sputtering was performed for more than 3 h to sufficiently remove a few tens nm thick oxide film. The temperature of the chamber was from 22−25°C during the pumping speed measurement.

The pumping speed of the titanium chamber is estimated as follows. The input gas flow rate Q_{in} is given by

$$Q_{in} = (P_{in} - P_{inBG})C_{SCE},$$

where P_{in} is the inlet gas pressure, P_{inBG} is the background pressure without gas input, and C_{SCE} is the conductance of the SCE. The SCE with C_{SCE} of 9.8×10^{-11} m^3 s^{-1} for N$_2$, which was calibrated by the National Metrology Institute of Japan, is used in the present experiment. The gas flow through the orifice from system 1 to system 2, $Q_{1 \to 2}$, is given as

$$Q_{1 \to 2} = C_o[(P_1 - P_{1BG}) - (P_2 - P_{2BG})],$$

where C_o is the conductance of the orifice, P_1 (P_2) is the pressure in system 1 (2), and P_{1BG} (P_{2BG}) is the background pressure in system 1 (2) without gas input. Then, the pumping speed of system 1, S_1, is written as

$$S_1 = \frac{Q_{in} - Q_{1 \to 2}}{P_1 - P_{1BG}} = \frac{Q_s}{P_1 - P_{1BG}}, \qquad (1)$$

where Q_s, defined as $Q_{in} - Q_{1 \to 2}$, is the gas flow pumped by the titanium chamber. C_o can be calibrated by the measurement as follows. When system 1 does not have the pumping speed for the input gas, Q_{in} equals $Q_{1 \to 2}$. Thus, C_o is given by

$$C_o = \frac{Q_{in}}{(P_1 - P_{1BG}) - (P_2 - P_{2BG})}. \qquad (2)$$

To confirm the validity of this throughput method, the pumping speed measurement with a commercial NEG pump (CapaciTorr® Z1000, SAES getter) was first performed. The NEG pump was installed instead of the electrode in system 1 in Figure 12. First, C_o was estimated by Eq. (2) without activation of the NEG pump. Table 2 shows the C_o values for several gas species. The estimated conductance using the transmission probability for round pipes, for example, Eq. (4.159) of Ref. 25, is 1.66×10^{-5} m^3 s^{-1} for N$_2$. This value agrees with the measured conductance within 7%. The calculated conductances C_{ocal}, which is the product of the measured C_o for N$_2$ and $(M_{N_2}/M_{gas})^{1/2}$, where M_{N_2} and

Table 2: Measured orifice conductance C_o, calculated conductance C_{ocal}, which is the product of C_o for N$_2$ and the square root of the mass ratio, are also shown.

Gas	C_o (m^3 s^{-1})	C_{ocal} (m^3 s^{-1})	C_o/C_{ocal}
N$_2$	1.8×10^{-2}	(1.8×10^{-2})	(1.0)
CO	1.8×10^{-2}	1.8×10^{-2}	1.0
H$_2$	5.8×10^{-2}	6.6×10^{-2}	0.89
O$_2$	1.8×10^{-2}	1.6×10^{-2}	1.1
Ar	1.2×10^{-2}	1.5×10^{-2}	0.85
CH$_4$	2.1×10^{-2}	2.3×10^{-2}	0.89

Table 3: Measured initial pumping speed S_{NEG} for the NEG pump, CapaciTorr® Z1000. Catalog values S_{NEGcat} are also shown.

Gas	S_{NEG} (m^3 s^{-1})	S_{NEGcat} (m^3 s^{-1})	S_{NEG}/S_{NEGcat}
N$_2$	3.2×10^{-1}	3.6×10^{-1}	0.89
CO	4.9×10^{-1}	5.5×10^{-1}	0.89
H$_2$	1.0	1.3	0.84
O$_2$	6.7×10^{-1}	7.0×10^{-1}	0.92
Ar	4.2×10^{-4}	0 (principal)	-
CH$_4$	1.7×10^{-4}	0 (principal)	-

M_{gas} are the mass of N_2 and a measuring gas, respectively, are also shown in Table 2. There are discrepancies between C_o and C_{ocal} is more than 10% except for CO. The reason would come from the error of the relative sensitivity. The pumping speeds of the NEG pump were measured after the activation, which was the 550°C baking for 2 h. Table 3 summarizes the measured initial pumping speed of the NEG pump S_{NEG} using Eq. (1) along with the catalog value S_{NEGcat}. The measured pumping speed agrees with the catalog value for all gas species. It is confirmed that the throughput method is valid for the pumping speed measurement.

B. Result of the sputtering and pumping speed

Figure 13 shows the result of the pressure in systems 1 and 2. After the system was evacuated by the TMP, the bake-out was performed at 200°C for degassing in point A. The gas injection line was also baked at about 100°C. As is the normal case, P_1 is larger than P_2. After the sputtering in point B, P_1 became smaller than P_2. This is clear evidence that the titanium chamber works as a getter pump. P_1 became even smaller by baking at 200°C after the sputtering at point C. Figure 14(a−c) shows residual gas spectra of system 1 at points α, β, and γ in Figure 13, respectively. The vertical axis is the ion current. As in Figure 4, the conversion factor of the RGA from the ion current of the corresponding mass number to the partial pressure was measured by introducing each gas with high purity. The conversion factors are 27 Pa A^{-1} for H_2 ($M/e = 2$), 34 Pa A^{-1} for CH_4 ($M/e = 15$), 38 Pa A^{-1} for CO ($M/e = 28$), 68 Pa A^{-1} for O_2 ($M/e = 32$), 54 Pa A^{-1} for Ar ($M/e = 40$), and 53 Pa A^{-1} for CO_2 ($M/e = 44$), respectively. It is noticed that the main residual gases after baking, such as H_2, H_2O, CO, and CO_2, are reduced by the sputtering. CH_4 does not decrease by the sputtering because it does not stick on titanium. Ar, which is the gas for the sputtering, increases. Ar is decreased by the
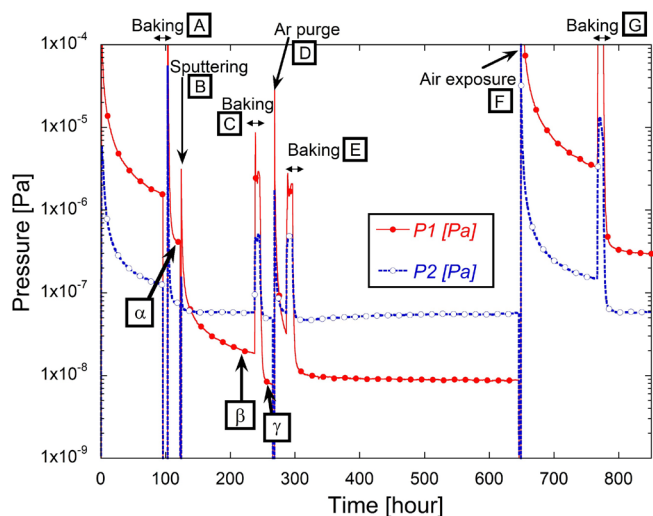

Figure 13: The trend of P_1 and P_2 in Figure 12, which shows the effect of the surface titanium-oxide film removal of the titanium chamber by the sputtering.
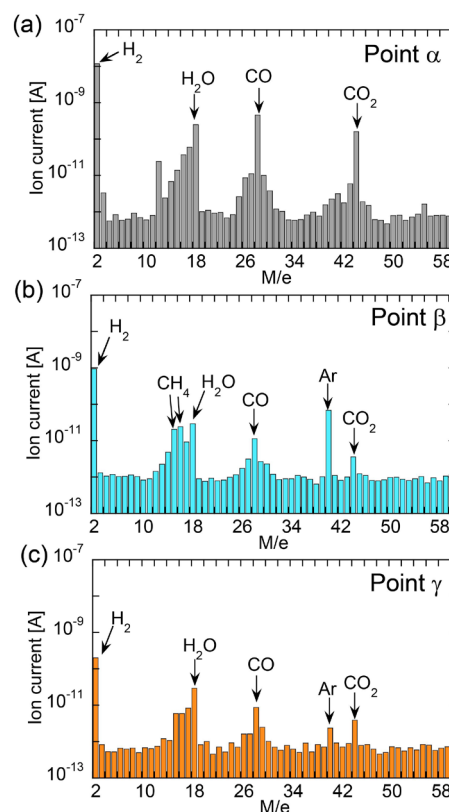

Figure 14: T Residual gas spectrum of the titanium chamber at (a) point α, (b) point β, and (c) point γ in Figure 13.

baking at point C. It is considered that Ar embedded during the sputtering in the titanium surface diffuses out by this baking. In the following process, the Ar gas was purged in the system to the atmospheric pressure at point D. The situation $P_1 < P_2$ can be kept after the re-pumping by the TMP without air exposure. This is because Ar does not react with the pure titanium surface. The baking at 200°C at point E makes P_1 smaller. However, once the chamber was exposed to the air at point F, the pressure P_1 did not become smaller than P_2 even by the baking at 300°C in point G. This is because the surface oxide film is immediately formed by the air exposure. The titanium chamber may partially have a getter function by the baking as demonstrated in the build-up test. It is considered, however, that the pumping speed is too small not to make P_1 smaller than P_2.

Table 4: Measured pumping speed for the sputtered titanium chamber S_{Ti}. The estimated value for the ideal clean titanium surface S_{Tical} is also shown.

Gas	S_{Ti} (m^3 s^{-1})	S_{Tical} (m^3 s^{-1})
CO	2.1	7.4
H_2	1.5×10^{-1}	2.3
O_2	3.1	7.8
CO_2	1.9	4.2
CH_4	7.2×10^{-4}	0 (principal)

The pumping speed of the titanium chamber was measured by the throughput method after the sputtering, which was the same condition as point β in Figure 13. Table 4 shows the measured pumping speed. The estimated pumping speed for the ideal clean titanium surface using the sticking coefficient [5] is also shown. The large pumping speed is obtained for H_2, CO, O_2, and CO_2, although they are smaller than that of the clean titanium surface deposited under ultra-high vacuum. The clear reason for this discrepancy is not exactly understood. One possibility is that the small amount of contaminated gas, such as H_2O or CO, is induced by argon sputtering, and they deteriorated the titanium surface. Another possibility may be that a part of the surface was not sputtered due to the distribution of the plasma and remained intact. The result that the pumping speed for CH_4 is almost zero is reasonable because it is not absorbed on the titanium surface.

IV. PREVENTION OF GETTER FUNCTION DETERIORATION BY AIR EXPOSURE AND ACTIVATION CYCLE

It has been shown in Section II that the titanium chamber gains some getter function by the high temperature baking due to the diffusion of oxygen in the surface titanium oxide into the bulk. However, the oxide remains on the surface even by the 400°C baking, and the carbide on the surface increases by the high temperature baking. In Section III, it was demonstrated that the titanium chamber works as a getter pump with a large pumping speed for several gas species by sputtering the surface oxide film. However, the electrode for the sputtering will be an obstacle in many devices, e.g., beam pipes of accelerators and a chamber for an emitter of an electron microscope. To remove the electrode, the chamber must be exposed to air, and the surface oxide film is again formed. In the previous research, Benvenuti et al. revealed that the increase of the activation temperature is effective to recover the sticking coefficient of the Ti-Zr-V
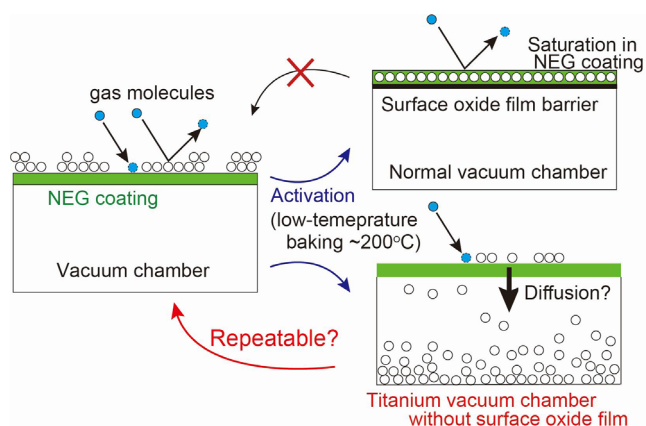
NEG coating [26]. Ono et al. [10] and Mase et al. [11] revealed that the oxygen-free titanium deposited stainless steel chamber maintains the getter function even after 30 times cycles of high-purity N_2 vent, air exposure, and activation. Inspired by these researches, we have started to develop a method to make a titanium chamber a getter pump by low-temperature baking after unmounting the electrode even when the air exposure and activation cycles are repeated. Figure 15 shows the idea of such a method. The NEG coating is usually formed on the surface oxide film of the vacuum chamber material, such as stainless steel, copper, aluminum, etc. Such an oxide film becomes a barrier against diffusing the NEG material oxide into the bulk when the NEG coating is activated. The problem is that the ratio of the oxide in the thin NEG coating becomes high by several times of air exposures and activations so that the sticking coefficient is decreased [26]. If the NEG coating is directly formed on the titanium surface, not on the titanium oxide film, the oxide of the NEG material may diffuse to the titanium bulk by the baking because there is no oxide film barrier between the NEG coating and titanium bulk. To achieve this situation, the NEG has to be coated in-situ after removing the surface titanium oxide film.

The experiment was performed with the same setup as Figure 12. The electrode was covered by a NEG alloy (Ti-Zr-V) tube, which was electrically connected to the electrode. The atomic composition of the NEG alloy was almost Ti : Zr : V = 1 : 1 : 1. This composition was measured by the inductively coupled plasma (ICP) mass spectrometry. The remaining alloy was chipped by the carbide drill to pieces of about 0.5 g and was measured by the ICP mass spectrometry. As shown in Figure 16, the titanium chamber surface was first sputtered with the electrode of a plus potential to remove the surface titanium oxide film, which was the same process as described in Section III.A. Then, the NEG was coated on the titanium surface by sputtering the NEG electrode cover. In this stage, the electrode potential was changed to the minus value to attract the Ar^+ ions. The bipolar power supply was used to perform this sputtering.

Figure 15: Assumed process of the repeatable activation when the NEG is directly coated on titanium with no surface oxide film.
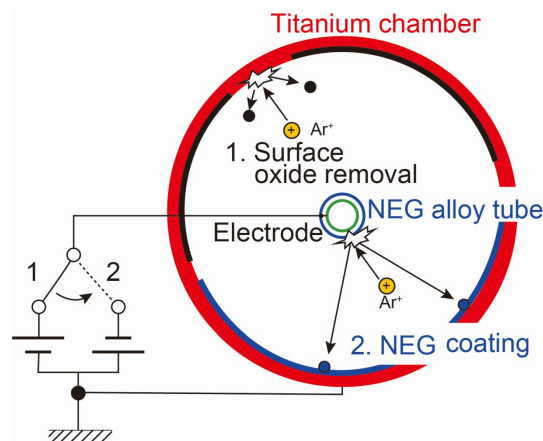

Figure 16: Sputtering method to coating the NEG film on titanium without a surface oxide film.
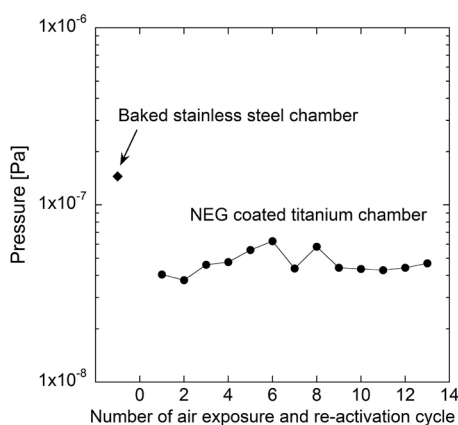
Figure 17: Pressure P_1 after the repeated air exposure and re-activation of the NEG coated titanium chamber. The final pressure of the stainless chamber with the same size baked several times at 200°C is shown for comparison.

The temperature of the titanium chamber was about 50°C in the surface oxide removal process and about 100°C in the NEG coating process. After these processes, argon was vented to the atmospheric pressure, and the system was exposed to the air to unmount the ICF152 flanges of the electrode with the NEG tube. The closing ICF152 flange was mounted after waiting 30 min with exposure to the air, and the system was evacuated by the TMP. The first activation was performed at 200°C for 8.5 h. After the system became room temperature, P_1 was measured. In practice, P_1, P_2, and the RGA spectrum were always acquired during the measurement. This was the first cycle of air exposure and activation. Then, the system was vented by the argon gas to the atmospheric pressure and exposed to the air by opening the closing ICF152 flange; the closing flange was mounted after waiting 30 min; the system was evacuated by the TMP; the second activation was performed; P_1 was measured after the system became room temperature. This was the second cycle. Figure 17 shows the pressure P_1 in each repeated air exposure and activation cycle. For comparison, the P_1 value of the stainless steel chamber with the same size as the titanium chamber was measured in the same setup after several times of the 200°C baking. The ultimate P_1 value for the stainless steel chamber is also shown in Figure 17. The pumping speed after the first air exposure and activation is shown as $S_{NC/Ti}$ in Table 5. The summary of the measured results is as follows; (1) The pumping speed for CO, H_2, and CO_2 are lower than that of sputtered titanium chamber, which is S_{Ti} in Table 4, while the pumping speed for O_2 is more than 3 m^3 s^{-1}. (2) The lower pressure than that of a baked stainless steel chamber is achieved for the surface sputtered titanium chamber with NEG coating. (3) The pressure does not increase by repeated air exposure and activation as expected.

Here, the pumping speed is compared with that of the previous NEG coatings. The Ti-Zr-V coating, which has been developed in CERN, has a pumping speed of 7×10^{-3}

Table 5: Measured pumping speed for the NEG coated titanium chamber $S_{NC/Ti}$ after the first air exposure and re-activation cycles. Estimated pumping speed for the NEG coating S_{CERN} and the oxygen-free palladium/titanium coating $S_{Pd/Ti}$ are also shown for comparison.

Gas	$S_{NC/Ti}$ (m^3 s^{-1})	S_{CERN} (m^3 s^{-1})	$S_{Pd/Ti}$ (m^3 s^{-1})
CO	2.3×10^{-1}	6.2	8.4×10^{-1}
H_2	2.9×10^{-2}	1.1×10^{-1}	6.7×10^{-1}
O_2	3.4	No data	No data
CO_2	3.5×10^{-1}	No data	No data

and 1.3×10^{-4} m^3 s^{-1} cm^{-2} for CO and H_2, respectively [25]. The oxygen-free palladium/titanium coating, which has been developed in High Energy Accelerator Research Organization (KEK), has a pumping speed of 9.5×10^{-4} and 7.5×10^{-4} m^3 s^{-1} cm^{-2} for CO and H_2, respectively [27]. The pumping speeds of these coatings, which are estimated for the surface area of the vacuum chamber used in this experiment, are also shown in Table 5. The pumping speeds for CO and H_2 of the present study are smaller than other coatings. Several reasons are considered for the lower pumping speed of the Ti-Zr-V deposited titanium chamber of this study. In the first stage of Figure 16, the titanium oxide on the chamber surface is sputtered and may coat the NEG electrode surface. Alternatively, oxygen in the titanium oxide surface could preferentially be sputtered and form the oxide of the NEG materials on the electrode surface. This is supported in the previous article, which reports the phenomenon that titanium oxide is reduced by ion sputtering [28]. After that, in the second stage, such oxides are also sputtered and coats the chamber surface. In such a case, the oxygen concentration in the NEG coating becomes high resulting in a lower pumping speed. The conditions during the NEG coating process are another possibility such as the chamber temperature, the surface roughness of the chamber, baking duration, etc. On the other hand, large pumping speeds are obtained for O_2 and CO_2, even though no comparable data for these gases were reported in other research. The development for obtaining a larger pumping speed for CO and H_2 is currently in progress.

V. CONCLUSION

Methods for making a titanium vacuum chamber a getter pump by removing the surface oxide film have been investigated. Surface oxide removal by baking has been examined by the build-up test. The high-temperature baking is effective to give some getter function on the titanium chamber. The vacuum firing makes the baking temperature lower than that without vacuum firing to obtain the same degree of activation. The surface and depth distribution analysis of the chemical composition by the XPS supports the build-up test result. Surface oxide film removal by the sputtering gives a large pumping speed for the titanium chamber. Once the chamber is exposed to the air, the getter function is lost due

to the reformation of the oxide film. To obtain a getter function by low-temperature baking after repeated air exposure and activation cycles, the NEG coating on the sputtered titanium would be effective because there is no oxide film barrier for the diffusion to the bulk between NEG coating and titanium bulk. The pressure keeps an almost constant value after the repeated air exposure and activation cycles. The development for obtaining a large pumping speed for major residual gases is ongoing.

Acknowledgments

References

[1] J. Kamiya, Y. Hikichi, M. Kinsho, N. Ogiwara, M. Fukuda, N. Hamatani, K. Hatanaka, K. Kamakura, and K. Takahisa, J. Vac. Sci. Technol. A **33**, 031605 (2015).

[2] H. Kurisu, T. Muranaka, N. Wada, S. Yamamoto, M. Matsuura, and M. Hesaka, J. Vac. Sci. Technol. A **21**, L10 (2003).

[3] N. Ogiwara, Proceedings of the 2nd International Particle Accelerator Conference (San Sebastián, 2011) pp. 971-975.

[4] J. Kamiya, J. Vac. Soc. Japan **59**, 213 (2016).

[5] D. J. Harra, J. Vac. Sci. Technol. **13**, 471 (1976).

[6] C. Benvenuti, P. Chiggiato, F. Cicoira, and Y. L'Aminot, J. Vac. Sci. Technol. A **16**, 148 (1998).

[7] C. Benvenuti, P. Chiggiato, F. Cicoira, and V. Ruzinov, Vacuum **50**, 57 (1998).

[8] C. Benvenuti, J. M. Cazeneuve, P. Chiggiato, F. Cicoira, A. Escudeiro Santana, V. Johanek, V. Ruzinov, and J. Fraxedas, Vacuum **53**, 219 (1999).

[9] T. Miyazawa, K. Tobishima, H. Kato, M. Kurihara, S. Ohno, T. Kikuchi, and K. Mase, Vac. Surf. Sci. **61**, 227 (2018).

[10] M. Ono, Y. Sato, Y. Masuda, T. Kikuchi, S. Ohno, Y. Nakayama, K. Mase, K. Ozawa, K. Yoshioka, and I. Yoshikawa, Proceedings of the 17th Annual Meeting of Particle Accelerator Society of Japan (Online, 2020) p. 350 (in Japanese).

[11] M. Ono, T. Kikuchi, K. Mase, Y. Masuda, Y. Nakayama, S. Ohno, K. Ozawa, Y. Sato, I. Yoshikawa, and K. Yoshioka, Proceedings of the 11th Mechanical Engineering Design of Synchrotron Radiation Equipment and Instrumentation (Chicago, 2021) pp. 119-122.

[12] K. Jousten, in, *Handbook of Vacuum Technology*, 2nd ed., edited by K. Jousten (Wiley-VCH, Weinheim, 2016) Chap. 11.

[13] J. Kamiya, Y. Hikichi, and K. Wada, Proceedings of the 16th Annual Meeting of Particle Accelerator Society of Japan (Kyoto, 2019) p. 1189 (in Japanese).

[14] J. Kamiya, K. Takano, H. Yuza, and K. Wada, Proceedings of the 12th International Particle Accelerator Conference (Campinas, 2021) pp. 3471-3474.

[15] L. Westerberg, B. Hjörvarsson, E. Wallén, and A. Mathewson, Vacuum **48**, 771 (1997).

[16] T. Hyodo and N. Mochizuki, J. MMIJ **123**, 698 (2007) (in Japanese).

[17] C.-C. Li, J.-L. Huang, R.-J. Lin, C.-H. Chen, and D.-F. Lii, Thin Solid Films **515**, 1121 (2006).

[18] L. Tenchine, X. Baillin, C. Faure, P. Nicolas, and E. Martinez, Procedia Eng. **5**, 359 (2010).

[19] T. Miyazawa, Y. Sugawara, I. Yoshikawa, Y. Sato, S. Ohno, T. Okada, M. Matsumoto, T. Kikuchi, and K. Mase, J. Vac. Sci. Technol. B **37**, 062923 (2019).

[20] J. Park, T. Back, W. C. Mitchel, S. S. Kim, S. Elhamri, J. Boeckl, S. B. Fairchild, R. Naik, and A. A. Voevodin, Sci. Rep. **5**, (2015).

[21] D. R. Baer, M. H. Engelhard, A. S. Lea, P. Nachimuthu, T. C. Droubay, J. Kim, B. Lee, C. Mathews, R. L. Opila, L. V. Saraf, W. F. Stickle, R. M. Wallace, and B. S. Wright, J. Vac. Sci. Technol. A **28**, 1060 (2010).

[22] D. Fernandes, E. Prokofiev, R. Valiev, A. Almeida, E. Monteiro, and C. Elias, Preprints 2018070464 (2018).

[23] C.-C. Li, J.-L. Huang, R.-J. Lin, D.-F. Lii, and C.-H. Chen, Thin Solid Films **517**, 5876 (2009).

[24] H. Yoshida, K. Arai, M. Hirata, and H. Akimichi, Vacuum **86**, 838 (2012).

[25] W. Jitschin, in, *Handbook of Vacuum Technology*, 2nd ed., edited by K. Jousten (Wiley-VCH, Weinheim, 2016) Chap. 4.

[26] C. Benvenuti, P. Chiggiato, P. Costa Pinto, A. Escudeiro Santana, T. Hedley, A. Mongelluzzo, V. Ruzinov, and I. Wevers, Vacuum **60**, 57 (2001).

[27] T. Miyazawa, Y. Kano, Y. Nakayama, K. Ozawa, T. Iga, M. Yamanaka, A. Hashimoto, T. Kikuchi, and K. Mase, J. Vac. Sci. Technol. A **37**, 021601 (2019).

[28] S. Hashimoto, Hyomen Kagaku **25**, 198 (2004) (in Japanese).